Available online at www.sciencedirect.com

ScienceDirect

Procedia Engineering 199 (2017) 1544–1549

Procedia Engineering

www.elsevier.com/locate/procedia

X International Conference on Structural Dynamics, EURODYN 2017

A match coefficient approach for damage imaging in structural components by ultrasonic synthetic aperture focus

S. Sternini[a,*], A. Quattrocchi[b], R. Montanini[b], A. Pau[c] and F. Lanza di Scalea[a]

[a] NDE&SHM Laboratory, Department of Structural Engineering, University of California, San Diego, 9500 Gilman Drive, La Jolla, CA 92O93, USA

[b] Università di Messina, Dipartimento di Ingegneria, Contrada di Dio, 98158 Sant'Agata, Messina, Italy

[c] Sapienza Università di Roma, Dipartimento di Ingegneria Strutturale e Geotecnica, Via Gramsci 53, 00197 Roma, Italy

Abstract

Ultrasonic Synthetic Aperture Focus (SAF) techniques are commonly used to image structural defects. In this paper, a variation of SAF based on ideas borrowed from Matched Field Processing (MFP) is evaluated to reduce artifacts and sidelobes of the resulting images. In particular, instead of considering the full RF ultrasonic waveforms for the SAF time backpropagation, only selected features from the waveforms are utilized to form a "data vector" and a "replica" (expected) vector of MFP. These vectors are adaptive for the pair of transmitter-receiver and the focus point. The image is created as a matched filter between these two vectors. Experimental results are shown for an isotropic and homogenous metallic plate with simulated defects, probed by six piezoelectric patches used as receivers or transmitters.

Peer-review under responsibility of the organizing committee of EURODYN 2017.

Keywords: Synthetic Aperture Focus; Ultrasonic Imaging; Matched Field Processing; Structural Health Monitoring.

1. Introduction

Synthetic Aperture Focus (SAF) is a common technique for ultrasonic imaging of defects in structural components [1]. Traditional SAF techniques use several transducers operated in a time backpropagation mode ("Delay-And-Sum") that essentially locates the reflector (discontinuity) by intersecting either ellipses (by tracking travel time between a transmission and a reception) or hyperbolae (by tracking travel time between receptions) [2].

* Corresponding author. Tel.: +1-619-415-7643.
E-mail address: ssternin@eng.ucsd.edu

1877-7058 © 2017 The Authors. Published by Elsevier Ltd.
Peer-review under responsibility of the organizing committee of EURODYN 2017.
10.1016/j.proeng.2017.09.503

SAF digital implementations were first proposed by Frederick et al. [3] and Jackson et al. [4]. Broadband impulse, direct data acquisition and coherent summation were adopted to show the feasibility of the digital SAF and to obtain a better evaluation of defects position, size and direction when applied to pressurized vessels. The classical SAF approach results in notorious sidelobes and, at times, artifacts: particular combinations of transmitter-receiver may produce poor correlation and therefore an erroneous reconstructed image [5]. Matched Field Processing (MFP) is used to locate acoustic sources in seismology and underwater acoustics [6]. In this case, a matched filter allows localizing acoustic sources by comparing the measured waves (data vector) with the expected responses at each point of the inspection volume (replica vector) [7]. The applied filter defines a "similarity" coefficient by means of a Matched Coefficient Approach (MCA) to quantify the relationship between the two vectors [8].

In this work we apply the general concept of MFP to ultrasonic SAF and demonstrate it for the imaging of simulated defects in a metallic plate. Specifically, instead of considering the full RF ultrasonic waveforms, only selected features from the waveforms are utilized to form the data vector and the replica vector. These features, that include time-of-flight and amplitudes, also account for multiple wave modes that can naturally propagate in the solid (L-wave and S-wave for a 3D geometry, and multiple guided waves for a waveguide geometry). This allows to combine, or compound, information from several sources to increase the contrast and focus of the resulting image, in analogy with multiple frequency compounding or multiple excitation compounding in biomedical imaging. The compounding generates "supervectors" for the measurements and the expectations. The correlation between "data supervector" and the "replica supervector" is estimated using a match filter correlation parameter that is based on a simple computation.

2. Experiments and imaging algorithm

2.1 Experimental setup

The experimental setup consisted of an isotropic and homogenous metallic plate with dimensions 762 × 940 × 3 mm, on which two holes of 13 mm diameter were drilled. A metal plank of 51 × 787 × 13 mm was glued with epoxy resin to simulate a stiffener, and two simulated clay defects of 38 mm in diameter were attached on the laminate surface. Six PZT patches (Physik Instrumente, DuraAct P-876.K025) were used as sensors and actuators and glued with epoxy resin on the surface of the plate. These transducers are composed by a piezoelectric layer of PIC255, a modified lead zirconate titanate, two electrodes, made of a conductive metal, and a polymeric case in Kapton. The dimensions are 17 × 13 × 0.5 mm. Mechanically, the PZT patches have a blocking force of 280 N, a minimum lateral contraction of 650 μm/m and an operating maximum frequency of 10^6 Hz; elastically, they show a capacitance of 8 nF, a voltage range during service of -100 to +400 V and a piezoelectric layer thickness of 200 μm. The expected fatigue resistance is up to 10^9 cycles and their operating temperature range is -20 to +150°C [9]. The PZT patches were connected to a data acquisition system NI PXI (National Instruments, mod. NI PXI-1033) with a function generator module (NI PXI-5412) and an amplifier (Peizo System, mod EPA-104-115) for the ultrasonic excitation phase. A digitizer module (NI PXI-5405) was used for the detection phase. Data post-processing was carried out using Matlab™.

2.2 Test procedure

The metallic plate was fixed by means of four dampers and the PZT transducers were placed as in Fig. 1. Two sinusoidal signals, Hanning-modulated in amplitude and consisting of 5 cycles at 120 kHz and 150 kHz, were used to drive the actuators for the wave excitation. The acquisition was carried out at 30 MHz with 15 averages. Each transducer was employed both as sensor and an actuator and the actuation was performed in a round-robin fashion("full matrix capture" mode of SAF). For each test, only one PZT patch at a time was transmitting the signal, while the other patches were recording the ultrasonic waves. Then the transmission was switched to a different patch and the test was repeated.

2.3 Imaging algorithm

The proposed algorithm allows identifying the location of defects and discontinuities on the surface of the metallic plate by tracking the travel time of the ultrasonic wave between a transmitter and a receiver. Six cycles with one actuator, changed between cycles, and five sensors were employed. The acquired signals were processed using a Hilbert transform in order to extract the envelope of the waveform, which facilitates peak extraction.

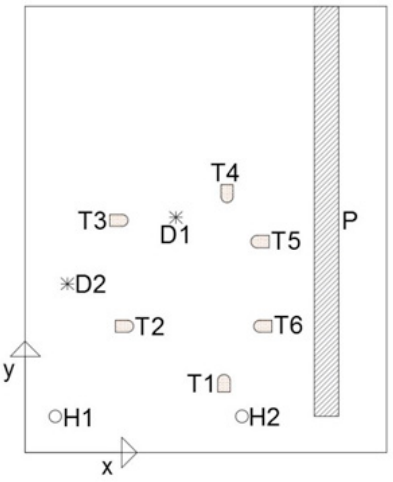

	x [mm]	y [mm]	notes
T_1	419	152	-
T_2	216	267	-
T_3	203	489	-
T_4	425	540	-
T_5	489	445	-
T_6	495	267	-
H_1	64	76	diameter = 13 mm
H_2	457	76	diameter = 13 mm
P	610 – 660	76 – 864	width = 51 mm
D_1	318	495	diameter = 38 mm
D_2	89	356	diameter = 38 mm

Fig. 1. Scheme of the experimental setup with transducers, holes, stiffener, and defect positions.

For each transmitter-receiver pair, one peak for each considered wave mode was extracted from the signal and used to create the data supervector, $\tilde{d}$. The expected travel time for all the pixel positions on the metallic laminate surface was also computed to build the replica supervector, $\tilde{m}_{xy}$. These vectors were compared by computing a matched coefficient β_{xy} ("similarity index"), defined in Equation 1.

$$\beta_{xy} = \frac{1}{1 + \left\| \tilde{d} - \tilde{m}_{xy} \right\|_1} \tag{1}$$

where $\left\| \tilde{d} - \tilde{m}_{xy} \right\|_1$ represents the L1 norm of the difference between data and replica supervectors and consequently the maximum absolute error between the two supervectors. This parameter associates an intensity value to every pixel in the image. In this way, when data supervector and replica supervector have a good similarity ($\tilde{d} \approx \tilde{m}_{xy}$), then $\beta_{xy} \approx 1$ and the pixel will have a high intensity. Conversely, if the two vectors do not match well, the parameter β_{xy} will be close to zero and the pixel will have low intensity.

2.4 Guided wave modes

Group velocities for the asymmetric mode A0 and for the symmetric mode S0 were evaluated in order to compute the travel time of the waves. In particular, the velocities were computed using dispersion curves for Lamb waves. Given the thickness of our plate, they were estimated as $c_g = 2200\ m/s$ for the A0 mode and $c_g = 4900\ m/s$ for the S0 mode at 120 kHz, and as $c_g = 2400\ m/s$ for the A0 mode and $c_g = 4900\ m/s$ for the S0 mode at 150 kHz.

3. Imaging results

The left and right columns in Fig. 2 show the comparison between reconstructed images of the metallic plate at 120 kHz and 150 kHz excitation, respectively. For each image, the blue dots represent the transducers, whereas the red ones represent holes, defects and the stiffener. On the x and y axes the distances from the origin are reported. A dB grey scale displays the value of $\boldsymbol{\beta}_{xy}$, where $\boldsymbol{\beta}_{xy}$ close to one corresponds to black (0 dB), and $\boldsymbol{\beta}_{xy}$ close to zero corresponds to white.

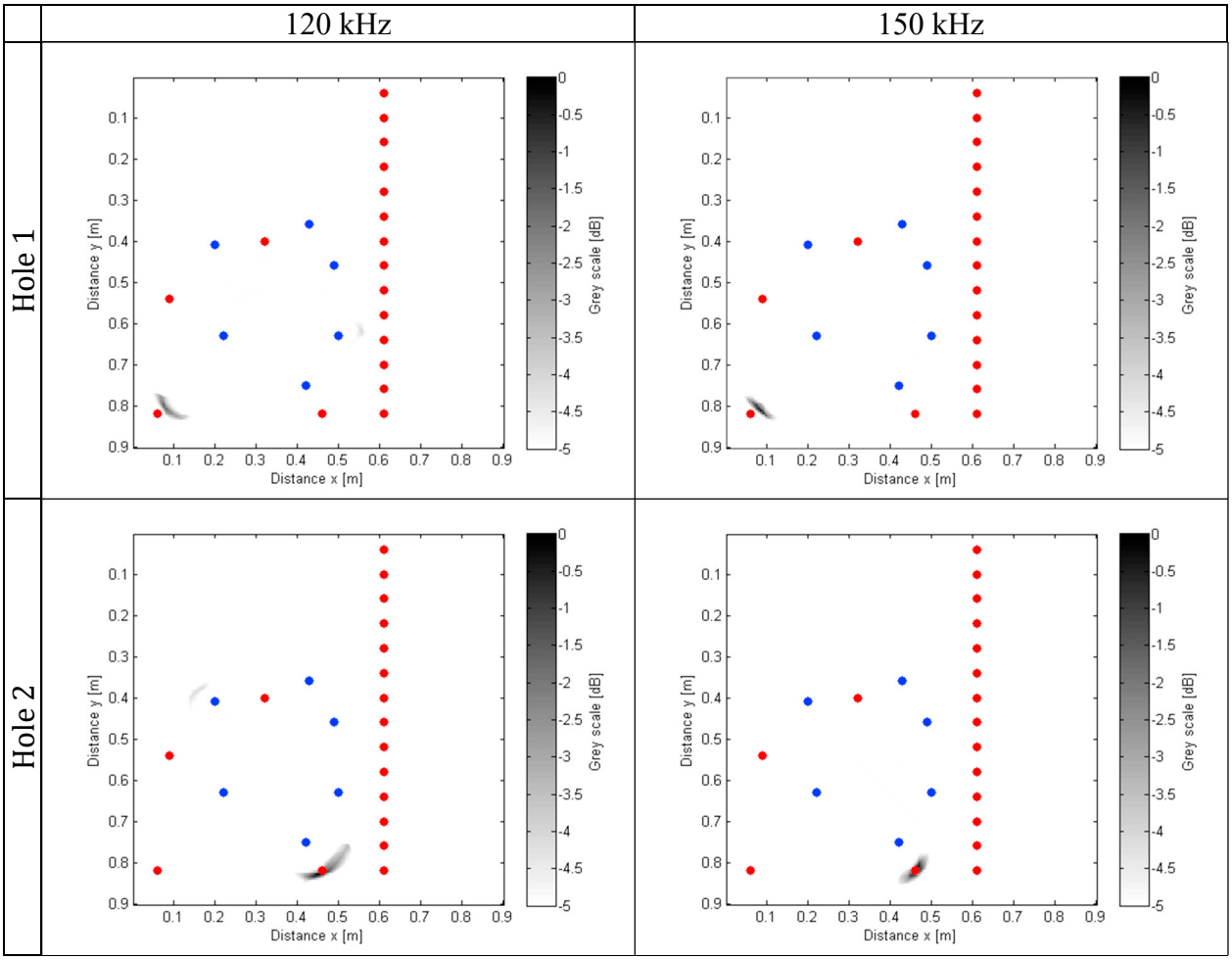

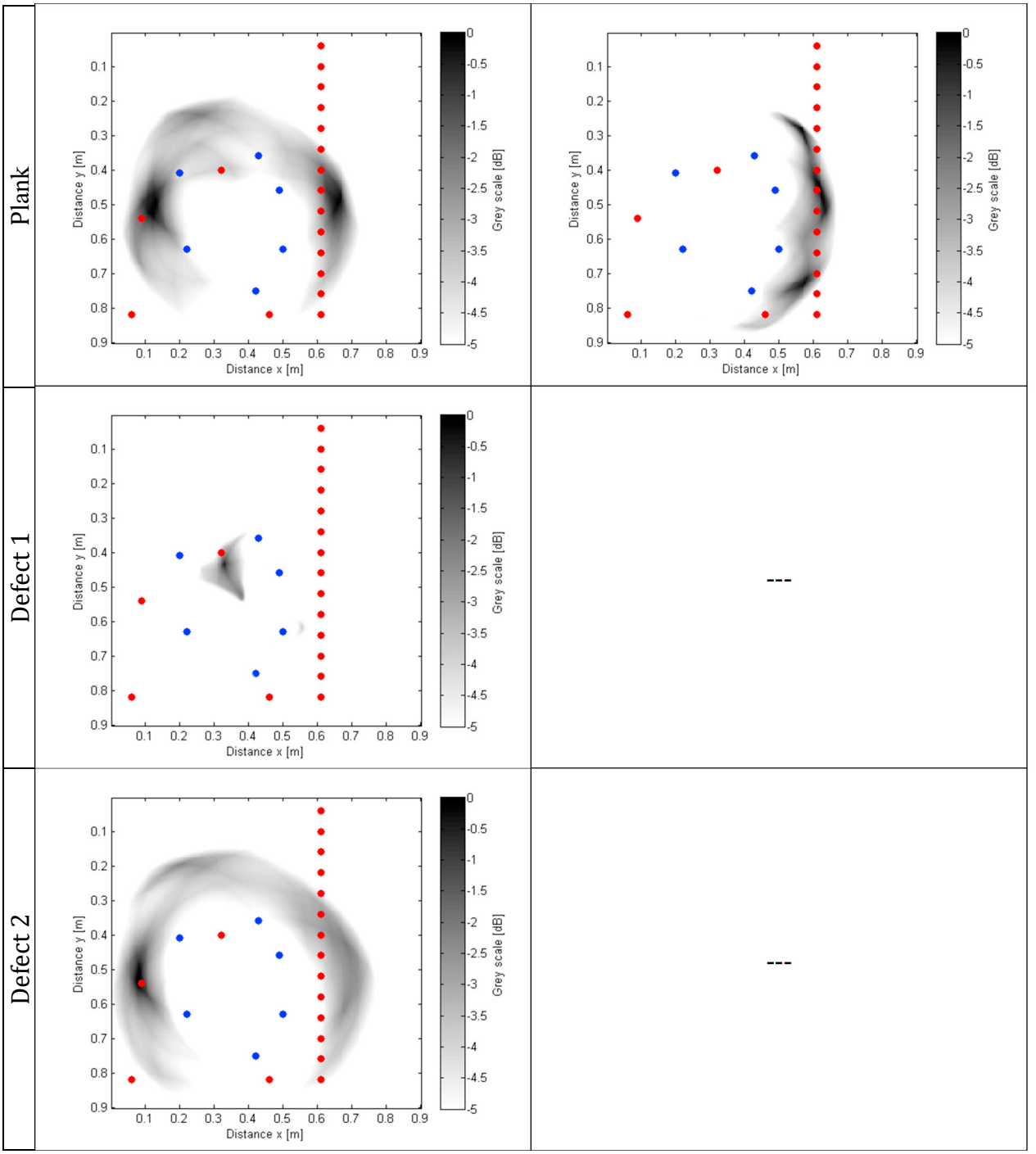

Fig. 2. Imaging results for matched field tests performed at 120kHz (left column) and 150kHz (right column). Detection of hole 1 (first row), hole 2 (second row), stiffener (third row), defect 1 (fourth row) and defect 2 (fifth row).

At the excitation frequency of 120 kHz, all discontinuities on target surface are detected. It is possible to see that the two holes are accurately located with almost no artifacts. The two simulated defects are also well identified. In

particular, defect 1 shows very little artifacts, whereas for defect 2 the algorithm shows a good simultaneous detection of the defect and the stiffener. A similar result is seen for the detection of the stiffener where also defect 2 was located.

Using the excitation at 150 kHz, the experiments were only performed considering the two holes and the stiffener. The two holes were still detected very accurately, with even lower sidelobes than the tests at 120 kHz. The stiffener was imaged through multiple reflections along its length and also in this case the higher frequency performs better than the lower frequency.

4. Conclusions

In this work an algorithm able to image defects and discontinuities on a metallic plate by means of modified synthetic aperture focus with matched coefficient approach has been proposed. Software implementation has been carried out by defining a correlation parameter to compare measured (data supervector) and expected (replica supervector) transmitter-receiver travel times and to associate this comparison to a pixel intensity scale. Two frequencies for the generation of ultrasonic waves were considered and their results presented. The proposed algorithm allows to detect and locate holes, defects and other elements present on the plate surface with good accuracy. The image computation is simpler and faster than backpropagating in time the entire RF waveforms. The approach also lends itself to considering several wave modes that propagate in the test medium (e.g. L and S waves for a bulk solid, or multiple guided waves in a waveguide [10]), and achieve improved focus by compounding this information. Additional work is needed to carry out a sensitivity analysis to determine the minimum defect size detectable by the proposed approach, as well as to compare the results with more traditional imaging approaches.

Acknowledgements

The research was supported by the joint project RESEARCH & MOBILITY 2015 funded by the University of Messina, Italy and by contract DTFR-5316C00024 (Dr. Robert Wilson, Program Manager) from the US Federal Railroad Administration.

References

[1] J. A. Jensen, S. I. Nikolov, K. L. Gammelmark, and M. H. Pedersen, Synthetic aperture ultrasound imaging, Ultrasonics, vol. 44, 2006, pp. e5–e15.

[2] V. Schmitz, S. Chakhlov, W. Müller, Experiences with synthetic aperture focusing technique in the field, Ultrasonics, vol. 38, issue 1, 2000, pp. 731-738.

[3] J. R. Frederick, C. Vanden Broek, S. Ganapathy, M. Elzinga, W. De Vries, D. Papworth, N. Hamano, Improved ultrasonic nondestructive testing of pressure vessels (No. NUREG/CR-0909). Michigan University, Ann Arbor, USA, 1979.

[4] J. L. Jackson, Program for field validation of the synthetic aperture focusing technique for ultrasonic testing (SAFT UT); analysis before test. Quarterly progress report. No. PB-286857, Southwest Research Inst., San Antonio, USA, 1978.

[5] S.I. Nikolov, J. Kortbek, Practical applications of synthetic aperture imaging, 2010 IEEE International Ultrasonics Symposium (IUS), San Diego, USA, 2010, pp. 350-358.

[6] W. A. Kuperman, G. Turek, Matched field acoustics, Mechanical systems and signal processing, vol. 11, issue 1, 1997, pp. 141-148.

[7] E. Jan, P. Svaizer, J. L. Flanagan, Matched-filter processing of microphone array for spatial volume selectivity, Circuits and Systems, ISCAS'95, 1995 IEEE International Symposium on., vol. 2, 1995, pp. 1460-1463.

[8] T. H. Gan, D. A. Hutchins, D. R. Billson, D. W. Schinde, The use of broadband acoustic transducers and pulse-compression techniques for air-coupled ultrasonic imaging. Ultrasonics, vol. 39 , 2001, pp. 181-194.

[9] A. Otto, P. Schittenhelm, K. Spanner, Piezoelectric actuator components, technologies, operation, Physik Instrumente (PI) GmbH & Co. KG, 2015.

[10] F. Lanza di Scalea, S. Sternini, T. V. Nguyen, Ultrasonic imaging in solids using wave mode beamforming, IEEE Transactions on Ultrasonics, Ferroelectrics and Frequency Control, DOI:10.1109/TUFFC.2016.2637299, December 2016, pp. 1-15.